Dyes and Pigments 99 (2013) 620–626

Contents lists available at SciVerse ScienceDirect

Dyes and Pigments

journal homepage: www.elsevier.com/locate/dyepig

# A ratiometric lysosomal pH chemosensor based on fluorescence resonance energy transfer

Jiangli Fan [a], Chunying Lin [a], Honglin Li [a], Peng Zhan [a], Jingyun Wang [b], Shuang Cui [b], Mingming Hu [a], Guanghui Cheng [a], Xiaojun Peng [a,*]

[a] State Key Laboratory of Fine Chemicals, Dalian University of Technology, No. 2 Linggong Road, High-tech District, Dalian 116024, PR China
[b] School of Life Science and Biotechnology, Dalian University of Technology, 2 Linggong Road, Dalian 116024, PR China

ARTICLE INFO

*Article history:*
Received 8 June 2013
Received in revised form
27 June 2013
Accepted 29 June 2013
Available online 13 July 2013

*Keywords:*
Naphthalimide–rhodamine
FRET
Ratiometric sensing
pH
Fluorescent sensor
Lysosome localization

ABSTRACT

In this work, we presented a naphthalimide–rhodamine based fluorescence resonance energy transfer system (FRET) **NR1** as a ratiometric and intracellular pH probe, in which 1,2,3-triazole was identified as an ideal bridge and biocompatibility. It could selectively monitor pH variations in methanol/HEPES solution at room temperature. When the pH changed from 6.20 to 2.00, both the fluorescence intensities at 580 nm and the intensity ratios, $R$ ($I_{580\ nm}/I_{538\ nm}$) increased, which allowed the detection of pH changes by both normal fluorescence and ratiometric fluorescence methods. The observation is consistent with the increased FRET from the 1,8-naphthalimide (donor) to the ring-opened, colored form of rhodamine (acceptor). Moreover, as **NR1** is lysosomal with low cytotoxicity, it will be helpful for investigating the pivotal role of $H^+$ in a biological context, especially in lysosomes through direct intracellular imaging.
© 2013 Elsevier Ltd. All rights reserved.

## 1. Introduction

Suitable intracellular pH ($pH_i$) [1] is critical for many tissue, cell and enzyme activities. However, abnormal $pH_i$ values are often associated with inappropriate cell function, growth, and division; and are observed in some common pathological states, such as cancers [2] and Alzheimer's disease [3]. Intracellular acidification is also an early feature of apoptosis. Thus, $H^+$ forms one of the most important targets among intracellular species.

In recent years, small fluorescent organic molecules, quantum dots and other nanoparticles [4–14] have been widely used for measuring pH changes in solutions or live cells. However, it is notable that there are only a few reagents for pH detection in weakly acidic environments. Moreover of these even fewer are cell membrane permeable, and so can monitor $H^+$ activities by cell imaging. In particular, since media such as those found in some organelles, e.g., endosomes and plant vacuoles with intracompartmental pH of 4–6, lysosomes with pH of 4.5–5.5, development of a wide variety of membrane-permeable "acidic" probes of high sensitivity and selectivity is desirable.

Most reported fluorescent pH sensors for live cells function by the enhancement of fluorescence signals. As the change in fluorescence intensity is the only detection signal, factors such as instrumental efficiency, environmental conditions, and probe concentration can interfere with the signal output. Accordingly, ratiometric sensors, which can eliminate most or all ambiguities by self calibration of two emission bands, are advantageous. Consequently, fluorescence (Förster) resonance energy transfer (FRET) is an optimal strategy, which can supply two fluorescence indicators (energy transfer donor and acceptor) [15,16]. In addition, the pseudo-Stokes shift of a FRET-based energy cassette is larger than the Stokes shifts of either the donor or acceptor dyes. This greatly reduces self-quenching, and fluorescence detection error due to the excitation backscattering effects.

Here, we present a naphthalimide–rhodamine FRET system **NR1** as a ratiometric and intracellular pH sensor. In recent years the strategy of connecting a shorter-wavelength fluorophore to a rhodamine spirolactam which can act as the energy acceptor has provided several ratiometric sensors based on ring-opening reactions induced by metal ions [17–19]. Furthermore, we chose naphthalimide as the energy donor since the emission spectrum of naphthalimide and the excitation spectrum of rhodamine B have substantial overlap, giving effective fluorescence energy transfer

* Corresponding author. Tel./fax: +86 411 84986306.
*E-mail address:* pengxj@dlut.edu.cn (X. Peng).

0143-7208/$ – see front matter © 2013 Elsevier Ltd. All rights reserved.
http://dx.doi.org/10.1016/j.dyepig.2013.06.032

with a single excitation wavelength. Given this molecular design, click chemistry provides a convenient synthetic method for uniting the two fluorophores, and the resultant 1,2,3-triazole was identified as an ideal bridge and biocompatibility [20,21]. Then, a $H^+$-induced process can change the emission maximum of the system from 538 nm (the characteristic peak of naphthalimide) to 580 nm (the characteristic peak of rhodamine). This wavelength shift allows the ratiometric detection of pH both in aqueous solution and live cells.

## 2. Experimental section

### 2.1. Apparatus and general methods

All solvents used were of analytical grade without further purification. $^1$H NMR and $^{13}$C NMR spectra were recorded on a VARIAN INOVA-400 spectrometer, using TMS as an internal standard. Mass spectrometry data were obtained with a HP1100LC/MSD mass spectrometer and a LC/Q-TOF MS spectrometer. UV–visible spectra were collected on a Perkin Elmer Lambda 35 UV–Vis spectrophotometer. Fluorescence measurements were performed on a VAEIAN CARY Eclipse Fluorescence Spectrophotometer with a slit width of 5 nm for excitation and 2.5 nm for emission, respectively. All pH measurements were made with a Model PHS-3C meter (SHANGHAI PRECISION & SCIENTIFIC INSTRUMENT CO., LTD). The fluorescence images of cells for the staining experiments were performed with an Olympus FV1000 confocal laser scanning microscope.

### 2.2. Synthetic routes of ***NR1***

#### 2.2.1. Synthesis of ***6***

According to the literature [22], compound **6** was synthesized by refluxing compound **7** and ethanolamine for 4 h in ethanol. After filtration, the crude product was recrystallized from ethanol as a white product with a yield of 70.3%. $^1$H NMR (400 MHz, $CDCl_3$), $\delta_H$ (ppm): 8.68 (d, 1H, $J = 8.0$ Hz), 8.60 (d, 1H, $J = 8.0$ Hz), 8.44 (d, 1H, $J = 4.0$ Hz), 8.06 (d, 1H, $J = 8.0$ Hz), 7.87 (t, 1H, $J = 8.0$), 4.46 (t, 2H, $J = 4.0$ Hz), 3.99 (t, 2H, $J = 4.0$ Hz). Q-TOFMS: $[M + H]^+$: 320.1432, found: 320.1430.

#### 2.2.2. Synthesis of ***5***

n-Butylamine (146.3 mg, 2 mmol) was added to compound **6** (160 mg, 0.5 mmol) in acetonitrile (30 mL), and the mixture refluxed at 90 °C for 20 h under nitrogen (TLC monitoring). After removal of acetonitrile and residual n-butylamine under vacuum, the residue was purified by flash chromatography with petroleum ether/ethyl acetate as eluent to give a bright yellow powder, compound **5** (122.13 mg, yield: 78.2%). TLC analysis: $R_f = 0.6$ in 50% ethyl acetate in petroleum ether. The structure of compound **5** was established by $^1$H NMR, $^{13}$C NMR, and MS [23].

#### 2.2.3. Synthesis of ***4***

Excess (1.0 mL) $PBr_3$ was added dropwise to compound **5** (60 mg, 0.19 mmol) in $ClCH_2CH_2Cl$ (10 mL). This was heated at 45 °C for 4 h. A little water was added to the mixture, which was then extracted with $CH_2Cl_2$ and dried over magnesium sulfate. After removal of solvent under vacuum, the residue was purified by flash chromatography with $CH_2Cl_2$ as eluent to give compound **4** as a bright yellow powder (17 mg, yield: 23.8%). $^1$H NMR (400 MHz, $CDCl_3$), $\delta_H$ (ppm): 8.56 (q, 1H), 8.45 (d, 1H, $J = 8.0$), 8.09 (t, 1H, $J = 4.0$), 7.59 (q, 1H), 6.70 (d, 1H, $J = 8.0$ Hz), 4.42 (t, 2H, $J = 4.0$ Hz), 3.64 (t, 2H, $J = 4.0$ Hz), 3.40 (t, 2H, $J = 8.0$ Hz), 1.80 (t, 2H, $J = 8.0$ Hz), 1.53 (q, 2H), 1.02 (t, 3H, $J = 8.0$ Hz). Q-TOFMS: $[M - H]^+$: 373.0796; found: 373.0627.

#### 2.2.4. Synthesis of ***2***

Compound **4** (100 mg, 0.27 mmol) and $NaN_3$ (87.75 mg, 1.35 mmol) were added to 20 mL ethanol. After heating at 110 °C for 24 h, the solvent was removed on a rotary evaporator. The resulting crude product was purified on a silica gel column with $CH_2Cl_2$/ethyl acetate as eluent to give compound **2** (54.08 mg, yield: 59.4%). $^1$H NMR (400 MHz, $CDCl_3$), $\delta_H$ (ppm): 8.56 (m, 1H), 8.44 (d, 1H, $J = 8.0$ Hz), 8.08 (t, 1H, $J = 4.0$ Hz), 7.59 (m, 1H), 6.69 (d, 1H, $J = 4.0$ Hz), 5.36 (s, 1H), 4.42 (t, 2H, $J = 8.0$ Hz), 3.64 (t, 2H, $J = 8.0$ Hz), 3.40 (m, 2H), 1.80 (m, 2H), 1.55 (m, 2H), 1.02 (t, 3H, $J = 8.0$ Hz), Q-TOFMS: $[M - H]^+$: 336.1465; found: 336.1526.

#### 2.2.5. Synthesis of ***1***

Rhodamine hydrazide **3** was synthesized from rhodamine B by the procedure published in literature [24]. Compound **3** (300.0 mg, 0.66 mmol), $K_2CO_3$ (96.6 mg, 0.7 mmol) was dissolved in 20 mL ethyl acetate in a 50 mL flask, excess (1.0 mL) 3-bromopropyne was then added dropwise with vigorous stirring. The mixture was refluxed overnight. After removal of ethyl acetate under vacuum, the residue was purified by flash chromatography with $CH_2Cl_2$/ethyl acetate as eluent to give compound **1** as a white powder (100 mg, yield: 30.6%). TLC analysis: $R_f = 0.6$ in 5.0% ethyl acetate in $CH_2Cl_2$. $^1$H NMR (400 MHz, $CDCl_3$), $\delta_H$ (ppm): 7.93 (t, 1H, $J = 4.0$ Hz), 7.47 (m, 2H), 7.11 (d, 1H, $J = 4.0$ Hz), 6.48 (d, 2H, $J = 8.0$ Hz), 6.41 (s, 2H), 6.28 (d, 2H, $J = 4.0$ Hz), 4.58 (t, 1H, $J = 8.0$ Hz), 3.33 (q, 8H), 3.32 (d, 2H, $J = 4.0$ Hz), 2.10 (s, 1H), 1.16 (t, 12H, $J = 8.0$ Hz). $^{13}$C NMR (100 MHz, $CDCl_3$), $\delta_C$: 166.79, 153.81, 151.90, 148.95, 132.90, 129.98, 128.44, 127.38, 124.11, 122.99, 107.97, 105.72, 98.11, 80.21, 72.54, 65.49, 44.47, 40.55, 12.76. Q-TOFMS: $[M + H]^+$: 495.2760; found: 495.2760.

#### 2.2.6. Synthesis of ***NR1***

Compound **2** (42 mg, 0.124 mmol) and compound **1** (61.29 mg, 0.124 mmol) were added to 10 mL DMF. After $CuSO_4 \cdot 5H_2O$ and sodium ascorbate (Sodium AC) were added to the solution, the mixture was stirred under $N_2$ at room temperature for 12 h. Excess water was added to the mixture, which was extracted with $CH_2Cl_2$ and dried over magnesium sulfate. After removal of solvent under vacuum, the residue was purified on a silica gel column with $CH_2Cl_2$/ethyl acetate as eluant to give **NR1** (74 mg, yield: 72.0%). $^1$H NMR (400 MHz, $CDCl_3$), $\delta_H$ (ppm): 8.48 (d, 1H, $J = 4.0$ Hz), 8.39 (d, 1H, $J = 8.0$ Hz), 8.15 (d, 1H, $J = 16.0$ Hz), 7.99 (d, 1H, $J = 14.0$ Hz), 7.52 (t, 1H, $J = 8.0$ Hz), 7.44 (t, 2H, $J = 8.0$ Hz), 7.08 (d, 1H, $J = 8.0$ Hz), 6.68 (d, 2H, $J = 8.0$ Hz), 6.59 (d, 2H, $J = 4.0$ Hz), 6.43 (s, 2H), 5.60 (s, 1H), 5.34 (s, 1H), 4.61 (d, 2H, $J = 4.0$ Hz), 4.54 (d, 2H, $J = 8.0$ Hz), 3.35 (q, 8H), 2.22 (t, 2H, $J = 8.0$ Hz), 1.77 (t, 3H, $J = 8.0$ Hz), 1.54 (q, 2H), 1.16 (t, 12H, $J = 8.0$ Hz). $^{13}$C NMR (100 MHz, $CDCl_3$), $\delta_C$: 175.60, 165.53, 164.45, 163.67, 152.57, 150.04, 149.05, 145.49, 134.93, 133.69, 131.46, 130.01, 129.90, 129.75, 128.84, 128.16, 127.37, 126.61, 124.56, 123.47, 122.25, 120.16, 109.10, 108.10, 104.95, 104.27, 98.41, 71.82, 65.53, 47.92, 44.34, 43.40, 39.30, 35.93, 31.92, 30.91, 29.70, 29.53, 29.34, 29.24, 29.13, 27.22, 25.54, 22.70, 20.35, 19.17, 14.14, 13.87, 12.63. Q-TOFMS: $[M + H]^+$: 830.4148; found: 830.4152.

### 2.3. FRET efficiency (E)

FRET efficiency can be obtained by measuring either the fluorescence intensities of the donor with and without an acceptor probe [25]. Thus

$$E = 1 - \frac{I_D}{I_{D0}}$$

where $I_D$ and $I_{D0}$ are the intensities in the presence and the absence of acceptor.

### 2.4. Theoretical calculations

The structures of **NR1** in the absence and presence of $H^+$ were optimized using density functional theory (DFT) by the B3LYP method with the 6-31G basis set. The DFT calculations were performed using the Gaussian 09 program.

### 2.5. pH bioimaging and lysosomes localization in MCF-7 cells

MCF-7 cells were cultured in Dulbecco's modified Eagle's medium (DMEM, Gibco; Invitrogen), supplemented with 100 units/mL penicillin, 100 g/mL streptomycin, and 10% heat-inactivated fetal bovine serum at 37 °C in a 5% $CO_2$ atmosphere. The cells were seeded on a Ø 35 mm confocal laser dish at a density of $2 \times 10^4$ cells $mL^{-1}$ in culture medium overnight. Then the MCF-7 cells were treated with 10 μM of **NR1** for 0.5 h and washed 3 times with prewarmed PBS (pH 7.20). To increase the concentration of cellular $H^+$, MCF-7 cells were treated with PBS (pH 4.45). Then the MCF-7 cells in different pH media were excited at 405 nm to obtain images with both white light and fluorescence, by using a digital color camera system (Olympus). To confirm the sensor's subcellular localization, acidic organelle specific lysosensor green was used to co-stain cells with **NR1**. MCF-7 cells were incubated for 30 min in the presence of lysosensor green (1 μM) and **NR1** (10 μM) simultaneously. The medium was removed, washed 3 times with prewarmed PBS (pH 7.20) and replaced with fresh medium. Cells were then analyzed with Olympus FV1000 confocal microscope. Images were obtained with both white light and fluorescence. Excitation wavelengths of lysosensor green and **NR1** were 488 nm and 405 nm respectively.

### 2.6. Measurement of cell viability

Cell viability was evaluated by the reduction of MTT (3-(4,5)-dimethylthiahiazo(-z-y1)-3,5-diphenytetrazoliumromide) to formazan crystals by mitochondrial dehydrogenases (Mosmann, 1983). Briefly, MCF-7 cells were seeded in 96-well microplates (Nunc, Denmark) at a density of $1 \times 10^5$cells/mL in 100 μL medium containing 10% FBS. After 24 h of cell attachment, plates were washed with 100 μL/well phosphate buffered saline (PBS) and then cells were cultured in medium with various concentrations (0, 1, 5 and 10 μM) of **NR1** and lysosensor green for 12 h. Cells in culture medium without **NR1** and lysosensor green were used as the control. Six replicate wells were used for each control and test concentration. 10 μL of MTT (5 mg/mL) prepared in PBS was added to each well and the plates were incubated at 37 °C for 4 h in a 5% $CO_2$ humidified incubator. The medium was then carefully removed, and the purple products were lysed in 200 μL dimethyl sulfoxide (DMSO). The plate was shaken for 10 min and the absorbance was measured at 405 nm and 488 nm using a microplate reader (Thermo Fisher Scientific). Cell viability was expressed as a percent of the control culture value.

## 3. Results and discussions

Both **1** [26] with a propagyl group and **2** with an azide group were efficiently synthesized and well characterized. Then, **NR1** was obtained easily by a click reaction between and **1** and **2** with 72.0% yield (Scheme 1). It was notable that this formation also contained an oxidative dehydrogenation of amine to imine moiety, which was a well known reaction in biochemistry promoted by coordination of

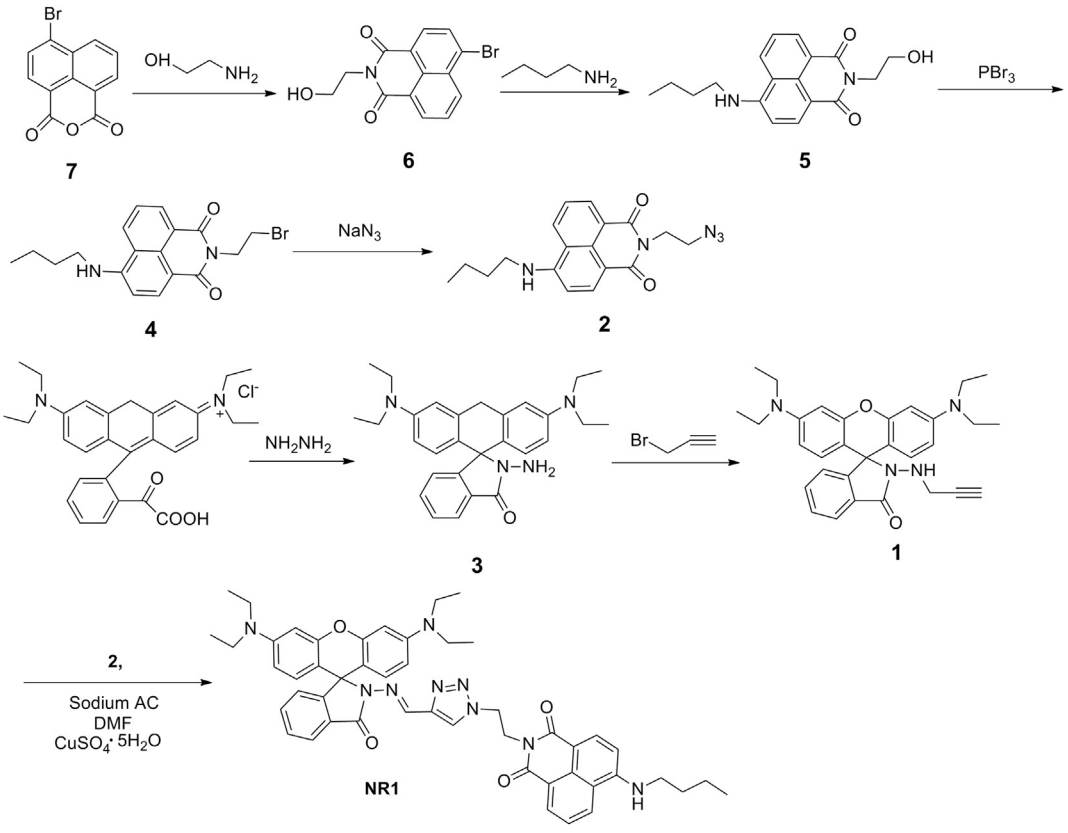


**Scheme 1.** The synthetic route of **NR1**.

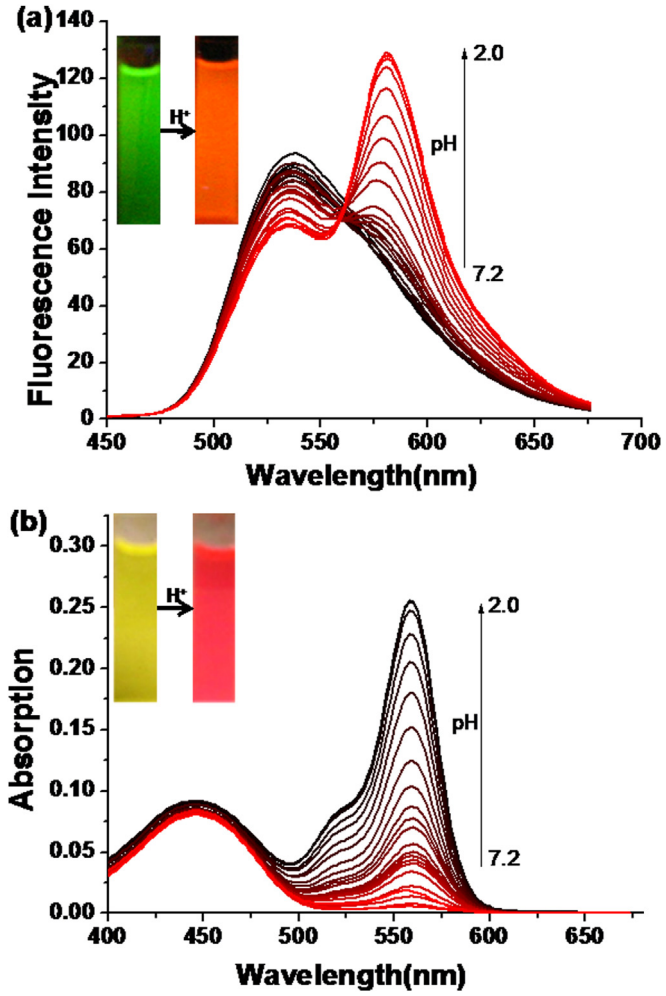


**Fig. 1.** Emission spectra of **NR1** (5 μM) at pH approximately range from 7.2 to 2.0 upon addition of HCl (1 M) in solution (methanol/HEPES = 9/1, v/v, pH 7.2). Inset: Change in fluorescence of **NR1** (5 μM) upon addition of $H^+$ (100 μM). Excitation wavelength is 430 nm. Slit: 5 nm/2.5 nm.

a transition metal cation such as $Cu^{2+}$ [27,28]. A peak of *m*/*z* 830.4148 in Q-TOFMS and the elemental composition of $C_{49}H_{52}N_9O_4$ suggested that this dehydrogenation reaction of amine group (Fig. S1). It was also confirmed by IR spectrum of **NR1**, in which a sharp band assigned to the C═N stretching vibrations at ca. 1636 $cm^{-1}$ (Fig. S2).

**NR1** is both hydrophilic and lipophilic, thus an optimized methanol/HEPES (9/1, v/v, pH 7.2) solution was selected as a testing system to investigate the optical response of **NR1** to pH at room temperature. **NR1** can instantly respond to a change of $H^+$ concentration and the resulting fluorescence is stable for a considerable time at pH 4.45 and 2.90 respectively (Fig. S3).

As shown in Fig. 1a, **NR1** showed green fluorescence and a yellow color when pH > 6.2, which was mainly ascribed to the optical properties of 1,8-naphthalimide. When the pH changed from 7.20 to 2.00, the intensity of the green fluorescent band centered at 538 nm gradually decreased and a new pink fluorescent band centered at 580 nm gradually increased. (Excitation wavelength is 430 nm) Accordingly, UV-absorption of the rhodamine moiety gradually increased, thus the solution of the probe underwent a distinct color change from yellow to pink, indicating that the probe **NR1** can serve as a "naked-eye" indicator for $H^+$ concentration (Fig. 1b). The observation is consistent with the increased FRET from the 1,8-naphthalimide (donor) to the ring-opened, colored form of rhodamine (acceptor). Both the fluorescence intensities at 580 nm (Fig. 1a) and the intensity ratios, $R$ ($I_{580\ nm}/I_{538\ nm}$) (Fig. S4) increased, which allowed the detection of $H^+$ by both normal fluorescence and ratiometric fluorescence methods. Actually, this took place mainly over the pH range 2.00–6.20, and the ratiometric calibration curve of $R$ ($I_{580\ nm}/I_{538\ nm}$) indicates the p*K*a is 2.79 (Fig. S4). This is mainly because the spirolactam ting of NR1 is "open" in the acidic conditions. The fluorescence ratio changes of **NR1** were fully reversible when it was treated with acid or base between pH 2.90 and 7.20 as shown in Fig. S5, which is of considerable potential for diagnosis and understanding of pathology.

To further discuss the FRET process between naphthalimide and rhodamine fluorophore, the structures of **NR1** before and after $H^+$-induced spirolactam ring open were optimized by Guassian 09 as shown in Fig. 2. Although the two distances between the donor and acceptor (1.31 nm and 1.01 nm) are similar, which are both in the range of 1–10 nm for FRET to occur, FRET only took place when the two fluorophores tended to parallel. So we speculated that the space arrangement between the energy transfer donor and acceptor also would influence the FRET or not. In this case, the FRET efficiency was 72%, that is why the fluorescence intensity of naphthalimide could not be quenched completely but ensured the double-wavelength emissions with ratiometric fluorescence detection of pH changes in live cells.

Considering that nitrogen and oxygen can bind to many metal ions in solution, it is important to determine whether non-$H^+$ ions were potential interferents. As shown in Fig. 3a, when keeping experimental conditions unchanged at pH 7.2, there was no obvious change of fluorescence ratio ($I_{580\ nm}/I_{538\ nm}$) upon the addition of

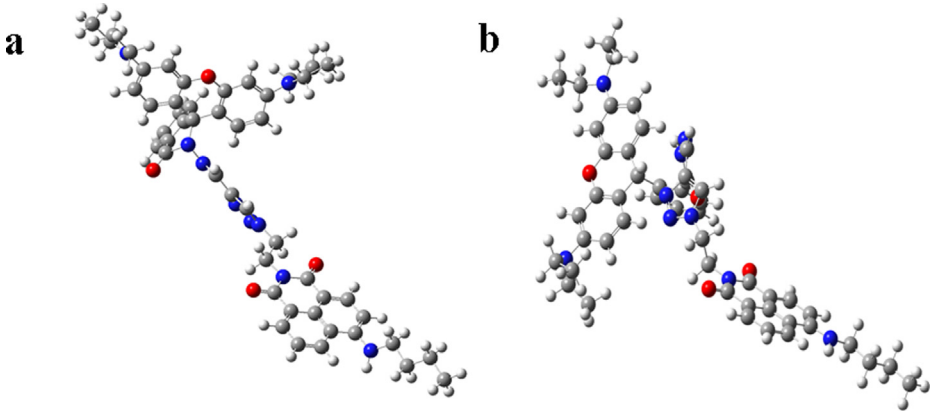


**Fig. 2.** The lowest energy structure of **NR1** in the absence (a) and presence (b) of $H^+$ by DFT calculations at B3LYP/6-31G (d, p) level.

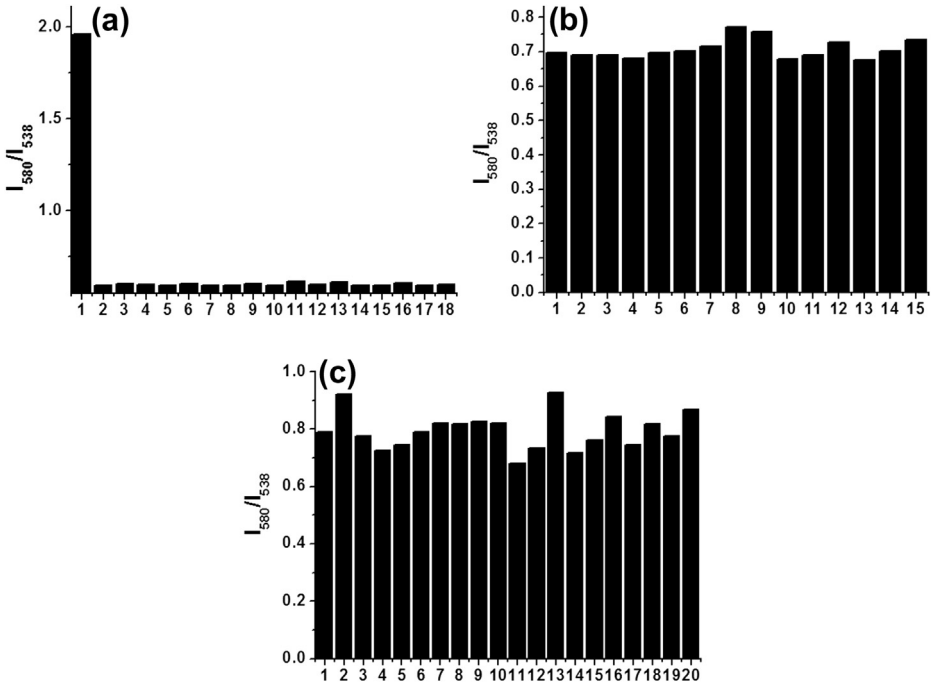


**Fig. 3.** (a) Selectivity of **NR1** for pH over selected cations interferences. The ratios of fluorescence emission intensity of **NR1** (5 μM) at 580 nm and 538 nm ($F_{580\ nm}/F_{538\ nm}$) containing various cations (333 μM) as compared to $H^+$ (200 μM) in the solution (methanol/HEPES = 9/1, v/v, pH 7.2). 1: $H^+$, 2: Blank, 3: $Na^+$, 4: $Ca^{2+}$, 5: $Mg^{2+}$, 6: $Zn^{2+}$, 7: $Cd^{2+}$, 8: $Ba^{2+}$, 9: $Fe^{3+}$, 10: $Fe^{2+}$, 11: $Cr^{3+}$, 12: $Pb^{2+}$, 13: $Cu^{2+}$, 14: $Hg^{2+}$, 15: $Mn^{2+}$, 16: $Ni^{2+}$, 17: $Co^{2+}$, 18: $NH_4^+$. (b) The ratios of fluorescence intensity of **NR1** (5 μM) at 580 nm and 538 nm ($I_{580\ nm}/I_{538\ nm}$) in the absence or presence of 333 μM above cations in the solution (methanol/HEPES = 9/1, v/v) at pH 4.45. 1: blank, 2: $Na^+$, 3: $Ca^{2+}$, 4: $Mg^{2+}$, 5: $Zn^{2+}$, 6: $Cd^{2+}$, 7: $Ba^{2+}$, 8: $Fe^{2+}$, 9: $Pb^{2+}$, 10: $Cu^{2+}$, 11: $Hg^{2+}$, 12: $Mn^{2+}$, 13: $Ni^{2+}$, 14: $Co^{2+}$, 15: $NH_4^+$. (c) The ratios of fluorescence intensity of **NR1** (5 μM) at 580 nm and 538 nm ($I_{580\ nm}/I_{538\ nm}$) in the absence or presence of 100 μM miscellaneous amino acid in the solution (methanol/HEPES = 9/1, v/v) at pH 4.45. 1: blank, 2: Ala, 3: Ser, 4: Met, 5: Gln, 6: Val, 7: Arg, 8: Phe, 9: Pro, 10: Thr, 11: Lys, 12: Asp, 13: Ile, 14: Leu, 15: Glu, 16: Cys, 17: Tyr, 18: GSH, 19: Tau, 20: NEM. Excitation wavelength is 430 nm. Slit: 5 nm/2.5 nm. The pH of solution was adjusted by aqueous solution of HCl (1 M).

various metal ions. Similarly, in Fig. 3b at pH 4.45, it is seen that various metal ions did not interfere with the fluorescence ratio changes caused by $H^+$. Furthermore, as shown in Fig. 3c, to imitate the complexity of the intracellular environment, the effects of amino acids were also investigated at pH 4.45. Overall **NR1** showed a selective response to $H^+$ in the presence of metal ions or amino acids. Therefore, **NR1** can detect pH changes with high selectivity by means of the FRET strategy.

In the present case fluorescence images of MCF-7 cells clearly show the intracellular localization of **NR1**. The double-channel fluorescence images at 538 ± 15 nm and 580 ± 15 nm are shown in Fig. 4. At pH 7.20, MCF-7 cells incubated with **NR1** (10 μM) for 30 min at 37 °C showed green intracellular fluorescence at 538 ± 15 nm (Fig. 4b) and weak red intracellular fluorescence at 580 ± 15 nm (Fig. 4c). When cells were washed in phosphate-buffered saline (PBS) medium of pH 4.45 and then incubated for another 30 min, the green fluorescence intensity decreased (Fig. 4f) and the red fluorescence intensity increased obviously (Fig. 4g) in above two channels respectively. Co-localization experiments, using the lysosomal probe lysosensor green, show that the site of **NR1**

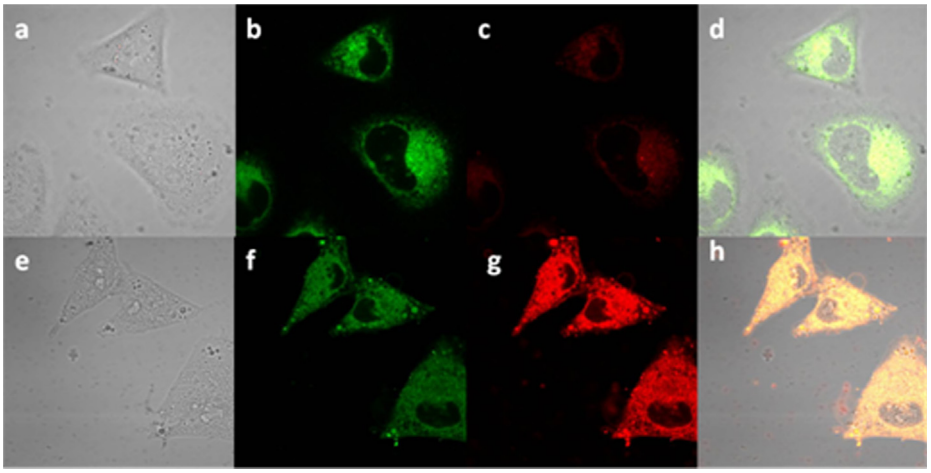


**Fig. 4.** Fluorescence mircoscope images of MCF-7 cells treated with probes **NR1** (10 μM) at pH 7.20 (a–d) and pH 4.45 (e–h), respectively. Bright field images (a and e), fluorescence images at channel I (538 ± 15 nm) (b and f), fluorescence images at channel II (580 ± 15 nm) (c and g), and the overlay images (d and h) of above (b and c) or (f and g). Excitation channel: 405 nm.

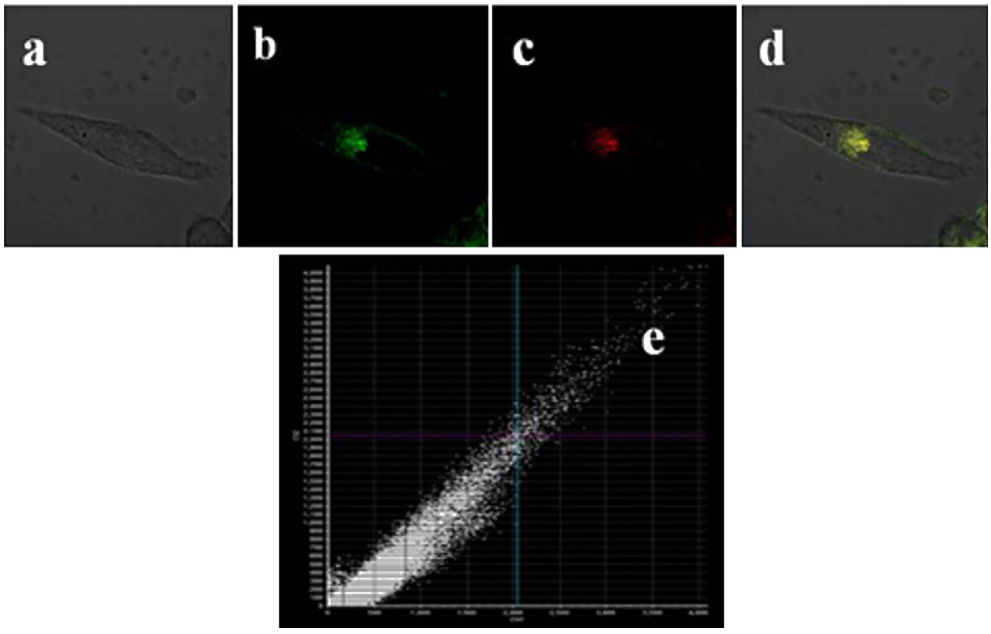


**Fig. 5.** Intracellular distribution of **NR1** (10 μM) as compared to lysosensor green (1 μM). (a) Bright field image; (b) fluorescence image of lysosensor green; (c) fluorescence image at 580 ± 15 nm of **NR1**; (d) merging of b and c; (e) co-localization coefficient of **NR1** and lysosensor green is 99.9% in the same cell. Excitation wavelength of lysosensor green and **NR1** respectively is 488 nm and 405 nm.

is lysosomal (Fig. 5). Lysosome is the first defense line of cells, capable of breaking down biological polymers and the lysosomal membrane had been considered to be the barrier of drug/DNA delivery. Thus **NR1** could provide ratiometric detection for intracellular pH, and could be a useful molecular sensor for studying biological processes involving $H^+$ within live cells.

Cytotoxicity of **NR1** to the above cell line was studied using Trypan blue staining (Fig. S6). After 12 h of cellular internalization of **NR1** and lysosensor green at different concentrations of 0, 1, 5 and 10 μM, respectively, more than 97% cells were viable, showing the non-cytotoxicity of **NR1** to cells at our experimental conditions.

## 4. Conclusions

In summary, we have developed a FRET-based ratiometric sensor **NR1** that can selectively monitor pH changes in the intensity ratio of the two strong emission bands of 1,8-naphthalimide and rhodamine. The significant changes in the fluorescence and color can be observed by eye. Moreover **NR1** is cell membrane permeable and localize in lysosomes. We consider that the highly sensitive pH fluorescent probe will be helpful for investigating the pivotal role of $H^+$ in a biological context, especially in lysosomes through direct intracellular imaging.

## Acknowledgments

This work was financially supported by NSF of China (21136002, 20923006, 21222605, 21272030, and 21076032), National Basic Research Program of China (2009CB724706 and 2013CB733702), National High Technology Research and Development Program of China (2011AA02A105) and Ministry of Education (NCET-12-0080).

## Appendix A. Supplementary data

Supplementary data related to this article can be found at http://dx.doi.org/10.1016/j.dyepig.2013.06.032.

## References

[1] Albert R, Walter FB. Intracellar pH. Physiol Rev 1981;61:296–434.
[2] Izumi H, Torigoe T, Ishiguchi H, Uramoto H, Yoshida Y, Tanabe M, et al. Cellular pH regulators: potentially promising molecular targets for cancer chemotherapy. Cancer Treat Rev 2003;29:541–9.
[3] Davies T, Fine RE, Johnson RJ, Levesque CA, Rathbun WH, Seetoo KF, et al. Non-age related differences in thrombin responses by platelets from male patients with advanced Alzheimer's disease. Biochem Biophys Res Commun 1993;194:537–43.
[4] Han J, Burgess K. Fluorescent indicators for intracellular pH. Chem Rev 2009;110:2709–28.
[5] Wang R, Yu C, Yu F, Chen L. Molecular fluorescent probes for monitoring pH changes in living cells. Trends Anal Chem 2010;29:1004–13.
[6] Best QA, Xu R, McCarroll ME, Wang L, Dyer DJ. Design and investigation of a series of rhodamine-based fluorescent probes for optical measurements of pH. Org Lett 2010;12:3219–21.
[7] Yuan L, Lin W, Cao Z, Wang J, Chen B. Development of FRET-based dual-excitation ratiometric fluorescent pH probes and their photocaged derivatives. Chem Eur J 2012;18:1247–55.
[8] Saha UC, Dhara K, Chattopadhyay B, Mandal SK, Mondal S, Sen S, et al. A new half-condensed Schiff base compound: highly selective and sensitive pH-responsive fluorescent sensor. Org Lett 2011;13:4510–3.
[9] Zhou X, Su F, Lu H, Senechal-Willis P, Tian Y, Johnson RH, et al. An FRET-based ratiometric chemosensor for in vitro cellular fluorescence analyses of pH. Biomaterials 2012;33:171–80.
[10] Park HJ, Lim CS, Kim ES, Han JH, Lee TH, Chun HJ, et al. Measurement of pH values in human tissues by two-photon microscopy. Angew Chem Int Ed 2012;51:2673–6.
[11] Saha K, Agasti SS, Kim C, Li X, Rotello VM. Gold nanoparticles in chemical and biological sensing. Chem Rev 2012;112:2739–79.
[12] Burns A, Ow H, Wiesner U. Fluorescent core-shell silica nanoparticles: towards "Lab on a Particle" architectures for nanobiotechnology. Chem Soc Rev 2006;35:1028–42.
[13] Tian M, Peng X, Fan J, Wang J, Sun S. A fluorescent sensor for pH based on rhodamine fluorophore. Dye Pigm 2012;95:112–5.
[14] Yang S, Ren C, Zhang Z, Hao J, Hu Q, Chen X. Aqueous synthesis of CdTe/CdSe core/shell quantum dots as pH-sensitive fluorescence probe for the determination of ascorbic acid. J Fluoresc 2011;21:1123–9.
[15] Kikuchi K, Takakusa H, Nagano T. Recent advances in the design of small molecule-based FRET probes for cell biology. Trends Anal Chem 2004;23(6):407–15.
[16] Fan J, Hu M, Zhan P, Peng X. Energy transfer cassettes based on organic fluorophores: construction and applications in ratiometric sensing. Chem Soc Rev 2013;42(1):29–43.
[17] Kim HN, Lee MH, Kim HJ, Kim JS, Yoon J. A new trend in rhodamine-based chemosensors: application of spirolactam ring-opening to sensing ions. Chem Soc Rev 2008;37:1465–72.

[18] Kim HN, Ren W, Kim JS, Yoon J. Fluorescent and colorimetric sensors for detection of lead, cadmium, and mercury ions. Chem Soc Rev 2012;41:3210–44.
[19] Fan J, Zhan P, Hu M, Sun W, Tang J, Wang J, et al. A fluorescent ratiometric chemodosimeter for $Cu^{2+}$ based on TBET and its application in living cells. Org Lett 2013;15:492–5.
[20] Ghosh KK, Ha HH, Kang NY, Yogeswari C, Chang YT. Solid phase combinatorial synthesis of a xanthone library using click chemistry and its application to an embryonic stem cell probe. Chem Commun 2011;47:7488–90.
[21] Meldal M, Tornoe CW. Cu-catalyzed azide-alkyne cycloaddition. Chem Rev 2008;108:2952–3015.
[22] Bojinov VB, Georgiev NI, Nikolov PS. J Photochem Photobiol A Chem 2008;193:129.
[23] Yuan D, Brown RG, Hepworth JD, Alexiou MS, Tyman JHP. The synthesis and fluorescence of novel N-substituted-1,8-naphthylimide. J Heterocycl Chem 2008;45:397–404.
[24] Yang X, Guo X, Zhao Y. Development of a novel rhodamine-type fluorescent probe to determine peroxynitrite. Talanta 2002;57:883–90.
[25] dos Remedios CG, Moens PDJ. Fluorescence resonance energy transfer spectroscopy is a reliable "ruler" for measuring structural changes in proteins: dispelling the problem of the unknown orientation factor. J Struct Biol 1995;115:175–85.
[26] Fan J, Lu J, Li H, Liu X, Zhu H, Peng X. An improved fluorescence-enhanced $Pd^{2+}$ probe derived from rhodamine fluorophore. Chin J Appl Chem 2011;28:1292–7.
[27] Keene RF. Metal-ion promotion of the oxidative dehydrogenation of coordinated amines and alcohols. Coord Chem Rev 1999;187:121–49.
[28] Wang D, Shiraishi Y, Hirai T. A BODIPY-based fluorescent chemodosimeter for Cu(II) driven by an oxidative dehydrogenation mechanism. Chem Commun 2011;47:2673–5.